

Two Ways of Walking: Contrasting a Reflexive Neuro-Controller and a LIP-Based ZMP-Controller on the Humanoid Robot ARMAR-4

Cornelius Goldbeck, Lukas Kaul, Nikolaus Vahrenkamp, Florentin Wörgötter, Tamim Asfour and Jan-Matthias Braun

Abstract—Full-size humanoid robots are traditionally controlled with the Zero Moment Point (ZMP)-paradigm and simplified dynamics, a well established method which can be applied to balancing, walking, and whole-body manipulation tasks. For pure walking control, approaches like pattern generators and reflexes are employed, often on optimized hardware. Both controller groups are developed on different platforms and therefore can only be indirectly compared in terms of human likeness or energy efficiency. We present a reflex based neuro-controller with an underlying, simple hill-type muscle model on the extremely versatile humanoid robot ARMAR-4. We demonstrate the reflexive controller’s flexible capabilities in terms of walking speed, step length, energy efficiency and inherent robustness against fall due to small slopes and pushes along the frontal axis. We contrast this controller with a Linearized Inverted Pendulum (LIP)-based ZMP-controller on the same platform. The promising results of this study show that even general humanoid robots can benefit from reflexive control schemes and encourage further investigation in this field.

I. INTRODUCTION

Based on the formulation of the *Zero Moment Point* (ZMP) introduced in the 1970’s as an elegant criterion for dynamic stability [1], numerous control methods for stabilizing dynamic gaits of bipedal robots emerged. ZMP-centered approaches for motion generation and control resulted in the first bipedal walking robots capable of dynamically stable gaits, like the early Honda robots [2]. These approaches rely on strict assumptions about the environment (e.g. flat ground), have rather low flexibility in terms of reacting to unforeseen disturbances, and tend to incur comparatively high costs of transport (CoT) [3]. Strong contributions to the field of ZMP-based walking have been made by Kajita et al. in the early 2000’s, where they made use of the simple yet very effective *Linear Inverted Pendulum Model* (LIPM) [4] and developed the successful ZMP preview-control [5].

In contrast to the efforts of using formal control methods and inspired by the elegance and efficiency of human gait, *Passive Dynamic Walkers* (PDW) were developed starting in the late 1980’s [6]. Typical for PDWs is their highly optimized mechanical structure that often includes springs, stops, and balance weights, which allows them to autonomously walk down slopes without a control system. The field of PDWs progressed towards *actuated* motion relying on minimal, reflex-based motor control and exploiting body dynam-

Cornelius Goldbeck, Lukas Kaul, Nikolaus Vahrenkamp and Tamim Asfour are with the High Performance Humanoid Technologies Lab, Institute for Anthropomatics and Robotics, Karlsruhe Institute of Technology (KIT), Germany asfour@kit.edu. Florentin Wörgötter and Jan-Matthias Braun are with the 3rd Physics Institute, Department of Computational Neuroscience, at the Georg-August-University, Göttingen, Germany janbraun@gwdg.de.

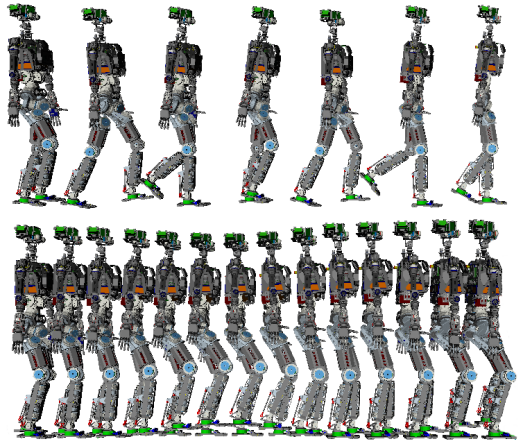


Fig. 1. Sequences of walking simulation snapshots under reactive control (top) and on a ZMP-controlled LIP-based generated trajectory (bottom). Note the significant difference in step length.

ics rather than overriding them with powerful control [7]. These kind of robots are currently the most energy efficient machines for bipedal walking [3].

Reflex-based motor control in actuated passive biped walkers draws inspiration from nature. Reflexes can be modeled as distributed neural circuits, generating motion commands as an immediate response to sensory feedback. Recent examples for neuro-inspired controllers include [8], [9], [10]. Another successful implementation of a neural walking controller for a real robot is the bipedal 2D walker RunBot [11]. RunBot, exploiting its specialized mechanical structure, achieved very high walking speeds under minimal neural control. Apart from their mere functionality, computational simplicity is another strong argument for the use of such reflex-based controllers.

Here, we present a novel, reflex-based, neuro-inspired walking controller for the full-sized humanoid robot ARMAR-4 [12] which has evolved from the RunBot control scheme. The controller has undergone some significant alterations to make it successful on the much more complex robot. We evaluate the gait properties produced by this controller in terms of speed, step length, and energy efficiency. We test the robustness of these gaits against external disturbances in the form of slopes and pushes to evaluate their passive stability.

As there are, to the best of our knowledge, no direct comparisons between ZMP and reflexive controllers on state of the art humanoids, we conclude the presented work contrasting the walking patterns obtained from the proposed controller

to classical, ZMP-controlled walking. All of our evaluation is conducted with a full dynamics simulator and a dynamic model of the ARMAR-4 robot (Fig. 1).

II. METHODOLOGY

A. Reactive walking controller for ARMAR-4

The reflexive control scheme for ARMAR-4 is based on the 2D bipedal walker RunBot [11] that consists of two legs and a very small trunk. Each leg has 2 active degrees of freedom (DoF) in the hip and the knee joints, and a passive compliant ankle joint. ARMAR-4 in contrast is a full humanoid with 63 DoF; more than 50% of the robot's 70 kg body mass are located above the hip. For ARMAR-4, we focus on the locomotion pattern and enforce 2D walking in the sagittal plane with external forces applied at the waist for lateral stability. The remaining challenge is balancing the upper body in direction of motion, which required several modifications to RunBot's original controller. In particular, the hip joints balance ARMAR-4's trunk, while knee and ankle joints control forward progression. Additional reflexes implement these changes, i.e., postural reflex, swing leg retraction, push-off, and swing initiation. Furthermore, the neuro-mechanical level was enhanced with compliant knee and ankle joints (Fig. 2).

1) *Neuro-Mechanics*: Joint torques τ_{joint}^i result from extensor and flexor motoneuron activities a ([11], Figs. 2, 3) or the passive torques of the spring-damper system in the knee (SDK) and ankle (SDA) joints

$$\tau_{\text{hip}}^i = \tau_{\text{hip}}^{\text{max}} \cdot (a_{\text{HF}}^i - a_{\text{HE}}^i) \quad (1)$$

$$\tau_{\text{knee}}^i = \begin{cases} \tau_{\text{SDK}}^i & \text{for } a_{\text{SI}}^i = 0 \\ I_a \cdot \tau_{\text{knee}}^{\text{max}} \cdot a_{\text{SI}}^i & \text{for } a_{\text{SI}}^i > 0 \end{cases} \quad (2)$$

$$\tau_{\text{ankle}}^i = \begin{cases} \tau_{\text{SDA}}^i & \text{for } a_{\text{PO}}^i = 0 \\ I_p \cdot \tau_{\text{ankle}}^{\text{max}} \cdot a_{\text{PO}}^i & \text{for } a_{\text{PO}}^i > 0 \end{cases}, \quad (3)$$

with $i \in \{\text{left}, \text{right}\}$, $\tau_{\text{joint}}^{\text{max}}$ the hardware torque limits, and the swing initiation (SI) and push-off (PO) reflexes. I_p , I_a are free parameters for scaling the reflex intensity. The spring-damper systems in the knee and ankle joints correspond to simple hill-type muscles and are implemented as variable Proportional-Derivative (PD) position controllers that generate the passive torques, with φ_j and $\dot{\varphi}_j$ denoting the local position and velocity of joint j :

$$\tau_i = P_j \cdot (\varphi_j^0 - \varphi_j) - D_j \cdot \dot{\varphi}_j \quad (4)$$

Human gait kinematics and torque curves [13] inspired the choices of the equilibrium point φ_j^0 , stiffness P_j , and the damping parameter D_j . They are encoded on the spinal reflex level and accessed by simple rules over sensory input. All remaining joints track their neutral positions with comparatively stiff PD-controllers.

2) *Reflex-Level Control*: Reflexes are implemented with a non-spiking neuron model that describes the average firing

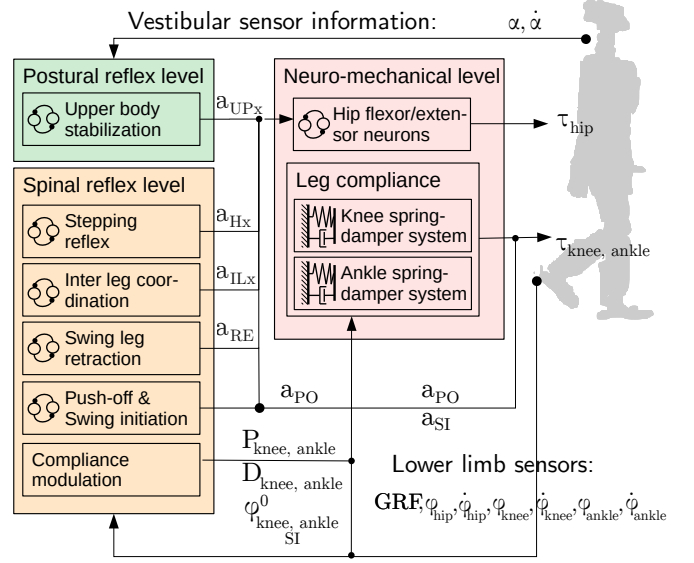


Fig. 2. Reflex activations a control joint torques at the lower limbs. Sensors include hip, ankle and knee joint angles φ , body orientation α , and ground reaction forces (GRF). P , D and φ^0 are the neuro-mechanical parameters of the spring damper systems (eq. (4)).

rate of neuron N as activity a_N

$$\frac{dy_N}{dt} = -y_N + \sum_Z \omega_{NZ} a_Z \quad (5)$$

$$a_N = \left(1 + e^{\beta_N (\Theta_N - y_N)} \right)^{-1}, \quad (6)$$

with membrane potential y_N , firing threshold Θ_N , and a positive constant β_N . Motoneurons are activated by the weighted (ω_{NZ}) sum of connected sensor- and inter-neuron-activity a_Z . Sensor neurons use the raw sensor value instead as membrane potential in equation (6) [11]. RunBot's controller network is still intact, but superimposed by any of the reflexes introduced in this paper.

The neural weights are noted in Fig. 3. The symmetric angle thresholds in $^\circ$ are $\Theta_{\text{HE}}^{\text{S}} = 205$, $\Theta_{\text{HF}}^{\text{S}} = 160$, $\Theta_{\text{RE}}^{\text{S}} = \Theta_{\text{HE}}^{\text{S}}$, $\Theta_{\text{IL}}^{\text{I}} = 0.6$, $\Theta_{\text{UP}}^{\text{S}} = 3$, $\Theta_{\text{GR}}^{\text{I}} = 5$, $\Theta_{\text{H}}^{\text{I}} = 5$, $\Theta_{\text{SW}}^{\text{I}} = -50$, $\Theta_{\text{ST}}^{\text{I}} = 100$, $\Theta_{\text{KN}}^{\text{S}} = 160$, $\Theta_{\text{A}}^{\text{S}} = 0.05$, $\Theta_{\text{SI}}^{\text{I}} = 2.9$, $\Theta_{\text{PO}}^{\text{I}} = 0.9$, with the superscript indicating sensor, inter-, and motoneurons. The constants β are set to 1, except for $\beta_{\text{HF}}^{\text{S}} = \beta_{\text{RE}}^{\text{S}} = -\beta_{\text{HE}}^{\text{S}} = 4$, $\beta_{\text{IL}}^{\text{I}} = \beta_{\text{A}}^{\text{S}} = \beta_{\text{SI}}^{\text{S}} = \beta_{\text{PO}}^{\text{S}} = 50$, $\beta_{\text{UP}}^{\text{I}} = 2.5$, and $\beta_{\text{KN}}^{\text{S}} = 5$.

Connectivity (weights), neuron thresholds, and parameters of the spring-damper systems provide the flexibility for adapting reflex-behavior or adjusting to changes in hardware.

The *inter leg (IL) coordination reflex* (Fig. 3) inhibits the ipsilateral extensor if the swing leg traverses the sagittal plane faster than the contralateral stance leg. Thus, CoM motion is stabilized and in-phase to leg swing. [14], [15] have shown a stabilizing effect of *swing leg retraction*, whereas [16] indicates an effective acceleration of the CoM. The corresponding reflex is triggered by a sensory neuron activated by the threshold Θ_{hip} exciting the ipsilateral hip flexor motoneuron (HF). We implemented a *push-off & swing initiation reflex*, powering leg swing by coupling

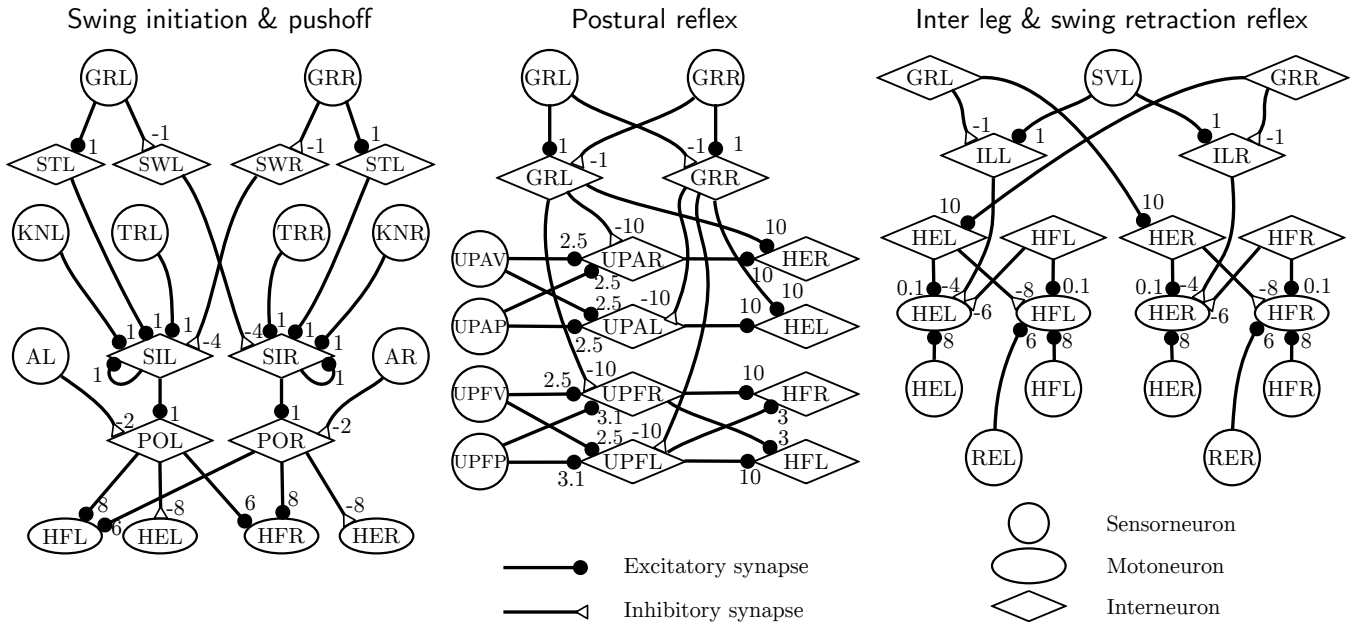


Fig. 3. Reflexes extending the RunBot-Controller [11]. The first letters label the neuron’s association: **H**ip Extensor/Flexor, **K**Nee, **A**nkle, **G**round contact, **S**wing **V**eLocity (angular velocity between the thighs), **U**Pper body, **P**ush-Off, **S**wing-Initialization, leg in **S**Wing or **S**Tance, and which leg is **T**Railing. The last letter indicates the side **L**eft/**R**ight, except for the upper body, where asymmetry in **V**elocity or **P**osition is tracked for **A**ft and **F**ore deviations. Synaptic weights ω are printed besides the synapses. Sensor neurons are active when the associated raw sensor crosses a threshold (eq. (6)), except for GRF, which is measured by absolute value. All other sensors are joint angles.

ankle plantar flexion and knee buckling [17]. The *Upper body stabilization reflex* processes the orientation α and the angular velocity $\dot{\alpha}$ of the upper body (UB) relative to gravity, balancing the trunk via excitation of hip flexor (HF) or extensor (HE) motoneurons in the stance leg.

B. Simulation environment

The reflexive and ZMP+LIPM controllers for ARMAR-4 were implemented for the ArmarX framework [18]. The dynamic simulation environment offers an interface to connect to the implemented controllers as well as a generic contact evaluation which computes the ground reaction forces. The multi-body dynamics as well as the solvers for the equations of motion are provided by Robotran [19].

C. ZMP preview control implementation

Our reference implementation of a ZMP controller closely follows the concepts presented in [20], [21]. With certain gait parameters like step length and duration specified, foot placements are computed and a ZMP trajectory is fitted to these placements. Simplifying the robot dynamics to those of a linearized inverted pendulum (LIP), a CoM trajectory is generated. According to foot placements and the CoM trajectory, a constrained inverse kinematics method produces whole-body motion. During motion execution, closed-loop control of the ankle torques is employed to keep the ZMP on its desired trajectory.

A major drawback with this approach is the constant height of the CoM that is inherently required by the LIP model. The inverse kinematics can only produce feasible robot motions that obey this restriction for comparatively

short steps. In contrast, the reflexive controller has no explicit constraints in step size.

III. RESULTS

3668 simulations were run to evaluate the gait patterns of the novel, reflexive controller with respect to selected properties like cost of transport, velocity, and step length. For these runs, we selected the following parameters for variation: push-off reflex intensity I_p and the ankle threshold angle Θ_p after which the push-off reflex is inhibited, both controlling power injection. The threshold for leg retraction Θ_{hip} regulating the step length, SDA parameters P_{ankle} and φ_{ankle}^0 prior to the application of plantar flexion moments, and the equilibrium point φ_{Torso}^0 of the Torso pitch joint that adjusts upper body leaning. The latter is thought to have a strong influence on walking speed [22].

Of the total number of 3668 runs, we tested 2093 parameter sets during a general screening of the parameter space, which provided 57 stable and 2036 unstable runs. Based on these results, smaller parameter spaces were investigated. For the cost of transport, 435 parameter sets were tested, including 115 stable runs; disturbances in form of a 2 m patch of slopes from $[-6, 6]^\circ$ and pushes along the frontal axis against the torso in the range of $[-80, 80]N$ were tested on the 57 stable gaits found in the initial screening. First, we will present the cost of transport and gait statistics of the presented controller, before we will continue to a compilation of these values for the ZMP controller. We will conclude this section by contrasting the two controllers’ characteristics.

TABLE I

EVALUATED PARAMETER RANGES IN WALKING EXPERIMENTS WITH THE PRESENTED CONTROLLER. RUNS 2-4 INCLUDE FOUR SELECTED SLOW WALKS WITH PARAMETERS LISTED IN 5

	$P_{\text{ankle}} \left[\frac{Nm}{c} \right]$	$\varphi_{\text{ankle}}^0 [^\circ]$	I_p	$\Theta_p [^\circ]$	$\Theta_{\text{hip}} [^\circ]$	$\varphi_{\text{Torso}}^0 [^\circ]$
1. Parameter screening: 2093 runs, 57 stable, 2036 unstable						
min	250	-0.2	0.2	-0.01	200	0
max	1000	0.2	1	0.05	208	0.2
2. Flat-ground walking: 435 runs, 115 stable, 320 unstable						
3. Slope walking: 684 runs, 93 stable, 591 unstable						
4. Pushes: 456 runs, 245 stable, 211 unstable						
min	250	-0.2	0.2	-0.01	200	0
max	850	0.2	1	0.05	208	0.2
5. Included 4 slow walks						
min	550	0.2	0.2	0.05	200	0
max	850					

A. Examination of the reflexive controller's gait-patterns

The examination of the obtained gait patterns was performed with variations in the ranges given in Table I, 1. Based on these screening runs, we determined the parameter ranges for the subsequent experiments and determined the gait stability criterion. In these experiments, a set of four very slow gaits was included for additional insight. The parameters of those four gaits are given in Table I, 5.

1) *Stability Criterion:* For a first classification, we decided to apply a run-time based stability criterion. The inherent instability of bipedal walking and the high number of ARMAR-4's degrees of freedom lets us assume that without additional control, we will have a non-diminishing rate of falls in simulations, independent of the run-time. Therefore, after tests with simulation run-times of 10 to 30 s, we investigated the distribution of falling times (Fig. 4). Assuming that the first peak at 10^3 ms is an artifact of the initial velocity, we fitted a log-normal distribution to the histogram with logarithmic binning. The fit according to equation (7) was performed with scipy [23]. Thus, we obtained the maximum likelihood estimates for the parameters to be $\sigma \approx 0.831$, $\mu \approx 596$ s, $\alpha = 3848$ s.

$$f(x) = \frac{1}{(x - \mu) \cdot \sqrt{2\pi\sigma^2}} \cdot e^{-\frac{\log(\frac{x-\mu}{\alpha})^2}{2\sigma^2}} \quad (7)$$

Based on these estimates, we assume to have eliminated more than 99.2% of all unstable gaits, when characterizing a stable gait by a run-time of at least 30 s.

2) *Achievable gait patterns:* The reflexive controller provides a diverse landscape of stable gaits with the parameter ranges shown in Table I. A variety of different speeds and stride lengths can be realized (Fig. 5a).

3) *Cost of transport:* The cost of transport (CoT, equation (8)) is a dimensionless variable, which can be used to compare the energy efficiency of locomotion. We use the mechanical work W performed in the joints of the lower limbs to transport the robot over the distance d :

$$\text{Cost of Transport (CoT)} = \frac{W}{g \cdot m \cdot d} \quad (8)$$

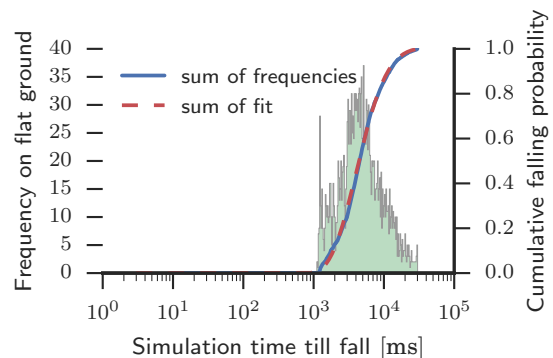


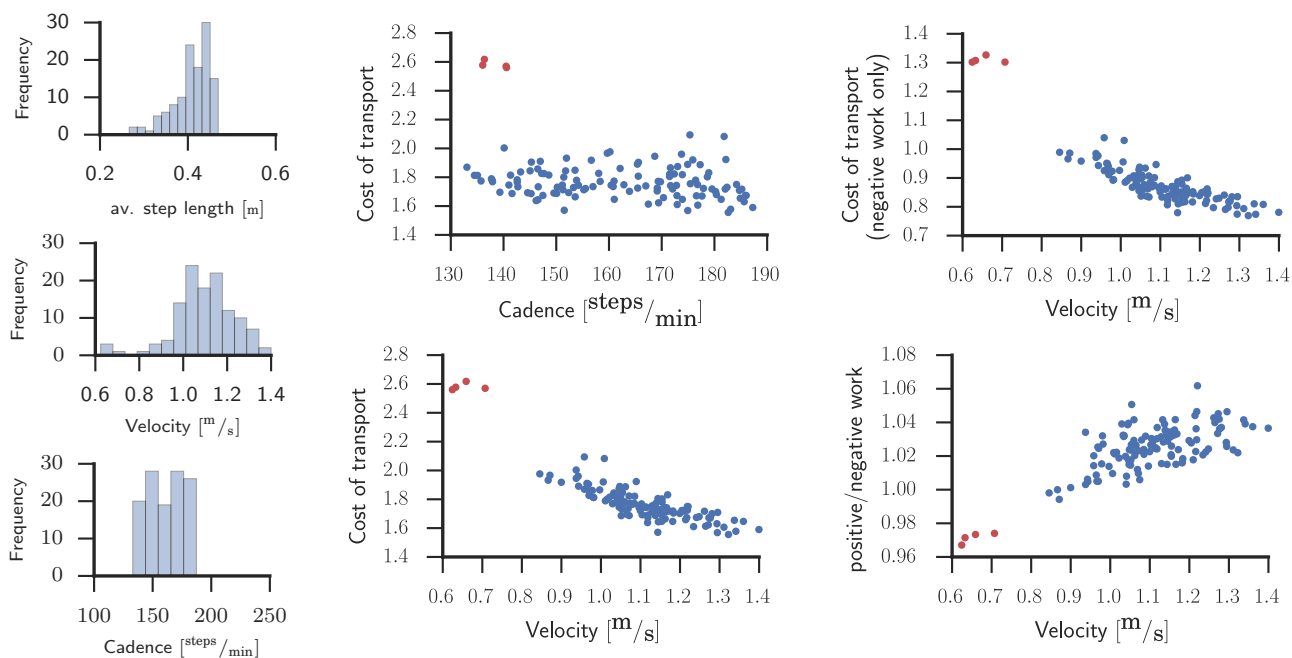
Fig. 4. Background: Distribution of falling times for unstable gaits from parameter space screening, assuming a 30 s stability criterion. The solid, blue line shows the cumulative distribution of falling times, the dashed, red line the log-normal fit which was used to estimate the ratio of missed unstable gaits to be below 0.8%.

with $m = 70$ kg and $g \approx 9.81$ m/s² for ARMAR-4 on earth. For an alternative definition, compare [3].

The CoT for the presented controller depends strongly on the chosen parameter set. In addition to the 57 stable gaits discovered during initial screening, we tested additional parameter sets according to Table I, 2.. This resulted in 115 stable gaits, for which we investigated the relation between gait characteristics, like cadence and velocity, and the energy efficiency of the controller. We find that the CoT in general does not change with the cadence (Fig. 5b, top), but changes strongly with the velocity, where higher velocities lead to lower CoT (Fig. 5b, bottom). Fig. 5c, top shows that the amount of negative work decreases with higher velocities. The negative work comes from motor torques opposing the current direction of joint rotation (i.e. active braking). While the absolute amount of positive work decreases, Fig. 5c, bottom indicates that the relative amount of negative work decreases, too. In other words, the reflexive controller is more energy efficient the less it brakes limb motions, and in effect, the faster is the resulting gait. The four slow gaits marked in red in Figs. 5b and 5c are obvious outliers.

4) *Robustness against small slopes:* In the first robustness experiment, the robot faces 2 m slopes of $[-6, 6]^\circ$ in a distance of 3.5 m from the starting point. In these trials, we tested the 57 stable gaits from the screening run. For these, Fig. 6 (left) shows per run the slopes the gait could master without falling during 20 s simulation time. The slopes each of the 57 stable gaits could master are shown in Fig. 7 (left). For the gaits in Fig. 6 (left), approximately 16% of the runs produced stable gaits and 11 gaits (19%) could not traverse any slope. 44 gaits (77%) successfully traversed 1 to 3 slopes, and only 2 gaits could withstand 4 and 5 slopes, respectively. This demonstrates that the property of robustness against slopes is very sensitive to the chosen parameters.

Additionally, we observe that the robot generally accelerates when walking downhill, whereas it gets slower when walking uphill. We want to emphasize here that the shown robustness against small slopes is a passive property of the selected gaits: it does not come from a dedicated stabilizing part of



(a) Stable gaits in parameter ranges of Table I demonstrate the flexibility of the reflexive controller's gait patterns.

(b) The cost of transport is decreasing with higher velocities, but seems mostly independent of the cadence. The four slow gaits are outliers with highly increased cost of transport and are marked in red.

(c) The ratio of work invested in accelerating over braking in the joints increases for higher velocities. The absolute amount of work against the joint motions decreases. Again, the slow gaits are separated and marked in red.

Fig. 5. Properties of the presented controller's gaits.

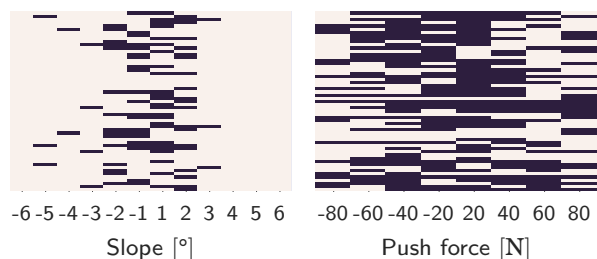


Fig. 6. **Left:** For the 57 parameter sets providing stable walking on flat ground found in initial screening, 27 were able to compensate for slopes. Slopes tested were in the range $-6 - 6^\circ$. The plot shows in dark colors for each of the 27 parameter sets on which slopes they were stable. A light color in the plot indicates falling due to the slope. **Right:** Stability against pushes in mid-swing is shown for 57 parameter sets providing stable walking on flat ground.

the controller. Learning experiments, e.g. [24], indicate that the passive robustness allows for the controller to adapt and therefore provides the foundation for further improvements.

5) *Robustness against pushes:* To test the robustness against pushes, the simulation was run for 20s: 10s to allow the influence of the initial condition to decay before a force (linearly ramped up and down within 0.5s) was applied against the root joint of ARMAR-4's torso with maximum push forces in the range of $[-80, 80]N$. The push-timing was fixed to mid-stance, when the swing leg traverses the stance leg.

Robustness against the tested pushes is more pronounced

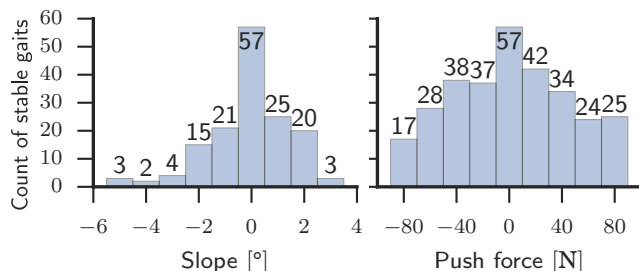


Fig. 7. **Left:** Count of stable parameter sets on slopes from $-6 - 6^\circ$ for 57 flat-ground stable parameter sets from initial screening. **Right:** Count of stable parameter sets when pushing with forces from $-80 - 80N$ for 57 flat-ground stable parameter sets from initial screening.

than against the tested slopes, with 54% stable runs overall (Fig. 6 (right) and Fig. 7 (right)). Of these, 40 (70%) walked stably for 4 – 6 push intensities. 11 gaits handled less than 3, and only 6 gaits more than 7 different push forces, with 3 gaits that were stable for all tested push forces. The controller seems to be largely invariant against the direction of the push, with 125 stable runs for positive push forces, and 120 for negative ones. From the 6 most robust gaits shown in Table II, the slow gaits seem especially resilient against pushes.

As with the robustness against small slopes, we want to emphasize here, that the robustness against pushes is a passive property. A stabilizing controller extending the presented design should be able to improve on the inherent

TABLE II

PARAMETER SETS OF THE SIX GAITS MOST STABLE AGAINST PUSHES IN THE TESTING RANGE OF $[-80, 80]N$ (FIG. 6). THREE OF THE FOUR VERY SLOW GAITS ARE REPRESENTED IN THIS TABLE AT ROWS 1, 3, 4. THE OTHER THREE MUCH FASTER GAITS SHOW SIMILAR PUSH-RESISTANCE

$P_{\text{ankle}} [Nm/c]$	$\varphi_{\text{ankle}}^0 [c]$	I_P	$\Theta_P [c]$	$\Theta_{\text{hip}} [c]$	$\varphi_{\text{Torso}}^0 [c]$	Stable against push forces $[N]$	#
850	0.2	0.2	0.05	200	0.0	-80, -60, -40, -20, 20, 40, 60, 80	8
350	-0.1	0.7	0.05	207	0.1	-80, -60, -40, -20, 20, 40, 60, 80	8
650	0.2	0.2	0.05	200	0.0	-80, -60, -40, -20, 20, 40, 60, 80	8
750	0.2	0.2	0.05	200	0.0	-80, -60, -40, -20, 20, 40, 60	7
250	0.1	0.4	0.05	204	0.0	-60, -40, -20, 20, 40, 60, 80	7
350	-0.1	0.9	0.025	207	0.05	-80, -60, -40, -20, 20, 40, 80	7

robustness demonstrated in this experiment. The chosen experimental setup focuses on the immediate response to the push, limiting the observation to short term reactions. We leave long time corrections of speed and walking direction after the push for additional higher-level control.

B. Contrasting the ZMP- and reflexive controller

While the reflexive controller demonstrated a versatile set of gaits, the linearized inverted pendulum is effectively limiting step sizes due to the requirement of a constant CoM height. As there are no explicit restrictions for the reflexive controller, a comparison of the two approaches is generally not straight-forward. We will therefore focus our attention on qualitative rather than quantitative aspects.

1) *Human Likeness*: The reflexive controller is designed to capture features like push-off and swing-leg retraction. Step lengths of up to 70 cm approach the range of adult humans with comparable leg lengths, which lies at 74 cm [25]. Although the typical step length of the presented controller is significantly smaller (Fig. 5a), it is generally much larger than that of the available ZMP controller (30 cm, see Fig. 1). The same holds for the walking velocity, with the ZMP controller providing 0.37 m/s and the reflexive controller achieving a typical velocity of more than 1 m/s (Fig. 5a).

2) *Energy Efficiency*: We only compare work done in the legs, as both our approaches do not make active use of any of the upper body actuators. The ZMP controller performed with $\text{CoT}_{ZMP} = 1.978$, while the reflexive controller's most energy efficient gait resulted in $\text{CoT}_{Ref} = 1.556$. Thus, the reflexive controller operates on the same hardware $\frac{\text{CoT}_{ZMP}}{\text{CoT}_{Ref}} = 1.27$ times more energy efficient.

3) *Robustness*: The stability against external forces over all gaits is much more symmetric for the reflexive controller (Fig. 7), whereas the ZMP stack had difficulties to compensate for pushes against walking direction, where it could only cope with -20 N . This might be due to the ZMP stack applying stabilizing moments only at the ankle joint level, which provides better levers in walking direction than against it due to the specific foot geometry.

IV. CONCLUSION

In this study we showed that the presented controller is capable of a variety of gaits with different step lengths and velocities. Fast gaits outperform the available ZMP based walking controller stack in terms of energy efficiency and walking speed. Some gaits show inherent robustness against

small slopes and pushes. Besides speed, energy efficiency, human-likeness and robustness, a major advantage of reflexive control over other methods is the computational parsimony. We explored the multi-dimensional parameter space of the controller and found promising sub-spaces that provide efficient, human-like, fast and robust gaits. In contrast to most reflex-based approaches in the literature, the presented controller does not depend on highly specific mechanisms. While this lack of specialized hardware may explain the rather low energy efficiency when compared to, e.g., [3], it allows to apply different controller architectures on the same robot.

It is a key contribution of this work to directly contrast a ZMP controller stack with a reflexive controller on the same humanoid. However, a general quantitative comparison is difficult to draw due to the differences between the two approaches: While the ZMP stack implements a 3D walker with an additional real-time stabilizer, the reflexive controller is effectively a 2D walker based on on-line motion generation and upper body stabilization. A disadvantage is the controller's limitation to steady walking without the ability to stand or move in confined spaces - situations that can be handled with ZMP-centered approaches. In summary, the reflexive controller is a major step towards exploiting the complete kinematic potential of the underlying ARMAR-4 platform.

As the selection of suitable sets of controller parameters poses a central problem, we aim at autonomously finding optimal parameter sets in terms of energy efficiency and robustness. Furthermore, a follow-up study might be concerned with the direct transition from one controller type to the other, leveraging the specific advantages (versatility and speed/energy efficiency) of both.

ACKNOWLEDGMENTS

This research has been supported by the German Federal Ministry of Education and Research (BMBF) under grant number 01GQ1005A and by the European Union's Seventh Framework Programme under grant agreement no. 611909 (KoroiBot).

REFERENCES

- [1] M. Vukobratovic and J. Stepanenko, "On The Stability of Anthropomorphic Systems," *International Journal of Mathematical Biosciences*, vol. 37, p. 1–37, 1972.
- [2] K. Hirai, M. Hirotsu, Y. Haikawa, and T. Takenaka, "The Development of Honda Humanoid Robot," in *1998 IEEE International Conference on Robotics and Automation (ICRA)*. IEEE, 1998, pp. 1321–1326.
- [3] P. A. Bhounsule, J. Cortell, A. Grewal, B. Hendriksen, J. D. Karssen, C. Paul, and A. Ruina, "Low-bandwidth reflex-based control for lower power walking: 65 km on a single battery charge," *The International Journal of Robotics Research*, vol. 33, no. 10, p. 1305–1321, 2014.
- [4] S. Kajita, F. Kanehiro, K. Kaneko, K. Yokoi, and H. Hirukawa, "The 3D Linear Inverted Pendulum Mode: A simple modeling for a biped walking pattern generation," in *IEEE/RSJ International Conference on Intelligent Robots and Systems*, 2001, p. 239–246.
- [5] S. Kajita, F. Kanehiro, K. Kaneko, K. Fujiwara, K. Harada, K. Yokoi, and H. Hirukawa, "Biped walking pattern generation by using preview control of zero-moment point," *2003 IEEE International Conference on Robotics and Automation*, p. 1620–1626, 2003.
- [6] T. McGeer, "Passive dynamic walking," *The international journal of robotics research*, vol. 9, no. 2, pp. 62–82, 1990.
- [7] S. Collins, A. Ruina, R. Tedrake, and M. Wisse, "Efficient bipedal robots based on passive-dynamic walkers," *Science*, vol. 307, no. 5712, p. 1082–1085, 2005.
- [8] J. H. Solomon, M. A. Locascio, and M. J. Hartmann, "Linear reactive control for efficient 2D and 3D bipedal walking over rough terrain," *Adaptive Behavior*, p. 1059712312462904, 2012.
- [9] N. V. der Noot, A. J. Ijspeert, and R. Ronsse, "Biped gait controller for large speed variations, combining reflexes and a central pattern generator in a neuromuscular model," in *2015 IEEE International Conference on Robotics and Automation (ICRA)*, May 2015, pp. 6267–6274.
- [10] Y. Huang and Q. Wang, "Torque-Stiffness-Controlled Dynamic Walking: Analysis of the Behaviors of Bipedes with Both Adaptable Joint Torque and Joint Stiffness," *IEEE Robotics Automation Magazine*, vol. 23, no. 1, p. 71–82, March 2016.
- [11] P. Manoonpong, T. Geng, T. Kulvicius, B. Porr, and F. Wörgötter, "Adaptive, fast walking in a biped robot under neuronal control and learning," 2007.
- [12] T. Asfour, J. Schill, H. Peters, C. Klas, J. Bucker, C. Sander, S. Schulz, A. Kargov, T. Werner, and V. Bartenbach, "ARMAR-4: A 63 DOF torque controlled humanoid robot," *2013 13th IEEE-RAS International Conference on Humanoid Robots (Humanoids)*, p. 390–396, 2013.
- [13] C. Kirtley, *Clinical gait analysis: theory and practice*. Elsevier Health Sciences, 2006.
- [14] M. Wisse, C. G. Atkeson, and D. K. Kloimwieder, "Swing leg retraction helps biped walking stability," in *5th IEEE-RAS International Conference on Humanoid Robots, 2005.*, Dec 2005, pp. 295–300.
- [15] D. G. E. Hobbelen and M. Wisse, "Swing-leg retraction for limit cycle walkers improves disturbance rejection," *IEEE Transactions on Robotics*, vol. 24, no. 2, pp. 377–389, April 2008.
- [16] T. R. Dillingham, J. F. Lehmann, and R. Price, "Effect of lower limb on body propulsion," *Archives of Physical Medicine and Rehabilitation*, vol. 73, no. 7, pp. 647–651, 1992.
- [17] S. W. Lipfert, M. Günther, D. Renjewski, and A. Seyfarth, "Impulsive ankle push-off powers leg swing in human walking," *Journal of Experimental Biology*, vol. 217, no. 8, pp. 1218–1228, 2014.
- [18] N. Vahrenkamp, M. Wächter, M. Kröhnert, K. Welke, and T. Asfour, "The Robot Software Framework ArmarX," *Information Technology*, vol. 57, no. 2, p. 99–111, 2015.
- [19] N. Docquier, A. Poncelet, and P. Fiset, "ROBOTRAN: a powerful symbolic generator of multibody models," *Mechanical Sciences*, vol. 4, no. 1, p. 199–219, 2013. [Online]. Available: <http://www.mech-sci.net/4/199/2013/>
- [20] S. Kajita, F. Kanehiro, K. Kaneko, K. Fujiwara, K. Harada, K. Yokoi, and H. Hirukawa, "Biped walking pattern generation by using preview control of zero-moment point," *2003 IEEE International Conference on Robotics and Automation*, p. 1620–1626, 2003.
- [21] S. Kajita, M. Morisawa, K. Miura, S. Nakaoka, K. Harada, K. Kaneko, F. Kanehiro, and K. Yokoi, "Biped walking stabilization based on linear inverted pendulum tracking," in *Intelligent Robots and Systems (IROS), 2010 IEEE/RSJ International Conference on*. IEEE, 2010, pp. 4489–4496.
- [22] S. Song and H. Geyer, "Regulating speed and generating large speed transitions in a neuromuscular human walking model," in *Robotics and Automation (ICRA), 2012 IEEE International Conference on*, May 2012, pp. 511–516.
- [23] E. Jones, T. Oliphant, P. Peterson *et al.*, "SciPy: Open source scientific tools for Python," 2001–, [Online; accessed 2016-07-14]. [Online]. Available: <http://www.scipy.org/>
- [24] P. Manoonpong and F. Wörgötter, "Efficiency copies in neural control of dynamic biped walking," *Robotics and Autonomous Systems*, vol. 57, no. 11, p. 1140–1153, 2009.
- [25] J. O. Judge, B. D. Roy, and S. Öunpuu, "Step length reductions in advanced age: the role of ankle and hip kinetics," *The Journals of Gerontology Series A: Biological Sciences and Medical Sciences*, vol. 51, no. 6, p. M303–M312, 1996.